Enhanced diffusion and non-Gaussian dynamics in driven magnetic nanoparticles

Ralph Lukas Stoop [1] and Pietro Tierno [1,2,3,*]

[1]*Departament de Física de la Matèria Condensada, Universitat de Barcelona, 08028 Barcelona, Spain*
[2]*Institut de Nanociència i Nanotecnologia, Universitat de Barcelona, 08028 Barcelona, Spain*
[3]*Universitat de Barcelona Institute of Complex Systems (UBICS), Universitat de Barcelona, 08028 Barcelona, Spain*

We investigate the out-of-equilibrium dynamics of paramagnetic colloidal nanoparticles driven above a triangular lattice of cylindrical ferromagnetic domains. We use an external precessing magnetic field to create a dynamic energy landscape which propels the particles along complex trajectories, characterized by an alternation of periodic orbital motion (localization) and stochastic particle jumping between nearest domains. We show that this system is populated by localized particles as well as delocalized (transported) ones, and tune their relative fraction via the field cone angle. Our driven system presents enhanced diffusive dynamics and an emergent non-Gaussian behavior which can be explained by considering two coexisting dynamic transport modes.

Introduction. The complex dynamics of particles driven through periodic potentials is common to many physical systems in condensed matter physics, spanning from charge density waves [1] to magnetotransport of electron gases [2–4], vortex matter in high T_c superconductors [5–7], skyrmions [8,9], and active matter systems [10]. Thus, describing and understanding the statistical properties of such systems is especially important for fundamental reasons. On the application side, the acquired knowledge can be also used to design logic devices based on the motion of interacting particles above periodic substrates [11–13]. Microscopic colloidal particles represent a versatile model system to investigate these general phenomena [14], since they have tunable interactions [15] and nowadays periodic potentials can be easily engineered on such a length scale [16–20]. Moreover, advances in chemical synthesis enable one to produce monodisperse and field responsive nanoparticles, which can be used to test these phenomena on smaller length scales, where thermal fluctuations play an important role.

An apparently unrelated phenomenon that has been reported in several soft matter systems [21–28] is the non-Gaussian diffusivity. This effect appears when a physical system displays a mean-square displacement (MSD) $\langle \Delta r^2 \rangle \equiv \langle |\boldsymbol{r}(t) - \boldsymbol{r}(0)|^2 \rangle$ linear in time t, $\langle \Delta r^2 \rangle = 2dDt$, where d is the system dimension and D the diffusion coefficient, while the displacement distribution, $G_s(r,t) \equiv \langle \delta(\boldsymbol{r} - |\boldsymbol{r}_i(t) - \boldsymbol{r}_i(0)|) \rangle$, is profoundly non-Gaussian. The surprise here comes from the fact that it is often assumed that non-Gaussian $G_s(r,t)$ would imply nondiffusive MSD, with $\langle \Delta r^2 \rangle \sim t^\alpha$ and an anomalous exponent $\alpha \neq 1$ [29,30]. This behavior was initially interpreted as the result of an exponential distribution of different diffusivities [31]. Another explanation provided later was based on assuming the presence of a dynamic environment, such that a tagged particle experiences a continuously changing environment [32,33]. This picture was placed in a general framework which reconciles the diffusing diffusivity model with a superstatistical description of the physical system [34]. We note that non-Gaussian displacement distributions have been also observed in the past in other systems [35], including glassy [36–38] or granular [39] materials. However, for microscopic particles driven above periodic potentials, MSD has been reported as superdiffusive [40] or ballistic [41], not normal ($\alpha = 1$), while the emergence of non-Gaussian statistics was observed for diffusing (not driven) particles confined above a plane [42–44].

In this Rapid Communication we experimentally demonstrate non-Gaussian diffusivity in a driven colloidal system, where paramagnetic nanoparticles are transported above a two-dimensional triangular lattice of cylindrical Bloch walls. We use a precessing magnetic field to modulate the stray field on the surface of a magnetic bubble lattice and realize a rotating energy landscape that forces the particles along complex trajectories characterized by a random switching between different orbital motions. We find that for a set of field cone angles, the dynamics are described by a linear MSD but a completely non-Gaussian displacement distribution. We note that larger particles driven across a bubble lattice were characterized by ballistic or localized trajectories but never diffusive ones [41]. The presence of strong thermal fluctuations weakens the pinning of the particles to the domain walls and generates a fraction of particles which are unable to follow the periodic magnetic modulation. Thus, our situation is similar to the case of molecules adsorbed and transported above a solid-liquid interface [45], although our system is further characterized by the driving field superimposed to the periodic substrate. Since many out-of-equilibrium effects observed with colloidal particles occur also in other condensed matter systems, such as vortex matter [46], we expect that our
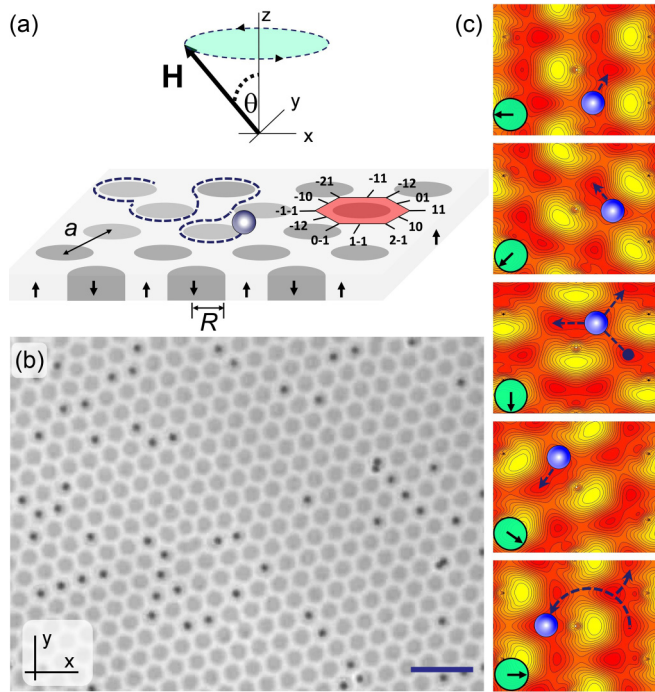
---

*ptierno@ub.edu

FIG. 1. (a) Schematic showing a paramagnetic nanoparticle driven above a magnetic bubble lattice by a precessing magnetic field with frequency ω and cone angle θ. One unit cell is highlighted in red with a schematic of the 12 possible directions. The basic vectors are $\boldsymbol{a}_\pm = (\sqrt{3}a/2, \pm a/2)$, where $a = 3.1\ \mu$m is the lattice constant, and gray circles illustrate the magnetic bubbles. (b) Polarization microscope image of the magnetic bubble lattice with a few paramagnetic colloids at zero external magnetic field ($H = 0$). The cylindrical domains (gray circles) are visible due to the polar Faraday effect; the scale bar is 10 μm. (c) Energy landscape of the bubble lattice calculated at an elevation $z = 0.37a$ (cone angle $\theta = 54.1°$) for $t = 0$ (top), $t = 0.3\pi/\omega, t = 0.5\pi/\omega, t = 0.8\pi/\omega$, and $t = \pi/\omega$ (bottom). Energy minima (maxima) are in red (yellow), and the schematic at the bottom indicates the direction of the in-plane rotating field H_{xy}.

results will be more general and can be applied to other driven systems through periodic potentials.

Experimental system. As colloids we use monodisperse paramagnetic nanoparticles of diameter $d = 540$ nm and magnetic volume susceptibility $\chi \sim 1$ (Microparticles PS-MAG-COOH). The particles are doped with iron oxide grains, and exhibit an induced magnetic moment $\boldsymbol{m} = d^3\pi\chi\boldsymbol{H}/6$ under the action of an external magnetic field $\boldsymbol{H}$. The particles are deposited above a triangular lattice (lattice constant $a = 3.1\ \mu$m) of cylindrical ferromagnetic domains, or "magnetic bubbles," located in a ferrite garnet film (FGF) [47] [see Fig. 1(a)]. The size of the domains can be controlled by an external field perpendicular to the film, $\boldsymbol{H} = H_z\hat{z}$. When $H_z = 0$ the domains have a radius $R = 1.2\ \mu$m, while for $H_z > 0$ ($H_z < 0$) their size reduces (increases) linearly as $R = a\sqrt{(H_z/M_s + 1)\frac{\sin(\pi/3)}{2\pi}}$, where $M_s \sim 10^4$ A/m is the saturation magnetization of the FGF. To drive the particles above the FGF, we use a precessing magnetic field which is obtained by using five magnetic coils. Two pairs of coils are arranged in a Helmholtz configuration and connected to a power amplifier (IMG STA-800) fed by a wave generator

(TTi TGA1244). An additional coil is placed below the FGF film to generate the static component H_z using a dc power supply (EL302RT, TTi). The custom-made coils are mounted on the stage of a polarization light microscope (Nikon, E400) equipped with a $100\times$, 1.3 numerical aperture (NA) objective. The particles are diluted in highly de-ionized water, so that above the FGF film their interactions are negligible, and we focus on the individual particle dynamics.[1] We use digital video microscopy [48] to track the positions $\boldsymbol{r}_i \equiv [x_i(t), y_i(t)]$ of N particles above the FGF, with $i = 1N$.

Particle transport. Once located above the FGF, the particles are pinned to the Bloch walls (BWs), which are located at the perimeter of the magnetic bubbles where the stray field of the FGF, $\boldsymbol{H}^s$ is maximal. As shown in Fig. 1(a), we modulate $\boldsymbol{H}^s$ and transport the particles across the lattice by using an external precessing magnetic field with a frequency ω and a cone angle θ with respect to $\hat{z}$,

$$\boldsymbol{H} \equiv H_0\{\cos\theta\hat{z} + \sin\theta[\cos(\omega t)\hat{x} + \sin(\omega t)\hat{y}]\}. \quad (1)$$

The applied field is composed of a rotating in-plane component of amplitude $H_{xy} = H_0\sin\theta$ and the out-of-plane one $H_z = H_0\cos\theta$, where the latter is used to control the width of the interstitial region between the bubbles. Throughout this work we mainly vary θ and keep the driving frequency fixed at $\omega = 4\pi\ \text{rad}\ \text{s}^{-1}$.

The sequence of images in Fig. 1(c) (from top to bottom) shows how the magnetostatic energy landscape is modulated during a half period of a precessing field with $\theta = 54.1°$ (details of the calculations can be found in Ref. [49]). As shown in the small schematic at the bottom of the top image, H_{xy} initially ($t = 0$) points along the $-1 - 1$ direction. As the field rotates, a particle trapped in one of the six energy minima (red wells) lags behind this minimum and may either circulate around a magnetic bubble or jump to another potential well of a nearest domain. This occurs at $t = 0.5\pi/\omega$, when three equidistant ($\sim a$) wells are nucleated close to the nearest bubbles, however, the minimum located along the $2 - 1$ direction is avoided by the particle as the sense of circulation follows the field chirality. From magnetostatic calculations we estimate that the height of the energy barrier connecting the equidistant minima can vary from $6k_BT$ to $20k_BT$, depending on the field cone angle [see Supplemental Material (SM) [50]], and can be surpassed by thermal fluctuations. The two possible paths after $t = \pi/\omega$ are shown in the bottom image of Fig. 1(c). Similar energy landscapes were observed for cone angles $\theta \in [45.1°, 83.6°]$, but not for the sole in-plane field $\theta = 90°$ (see below).

Results. To characterize the dynamical regimes we measure the MSDs for different values of the precession angle $\theta \in [42.1°, 90.0°]$ [see Fig. 2(a)]. For $\theta = 90°$ ($H_z = 0$) the in-plane field forces the particles to perform a rotational periodic motion around the bubbles [Fig. 2(b)]. Since the magnetic stray field of the circular domains has cylindrical symmetry, its perimeter is an equipotential circle. The in-plane field

---

[1]Before the experiments, the FGF is coated with a 1-μm-thick layer of a positive photoresist (AZ-1512, Microchem, MA) to prevent the particles from sticking to the domain walls.
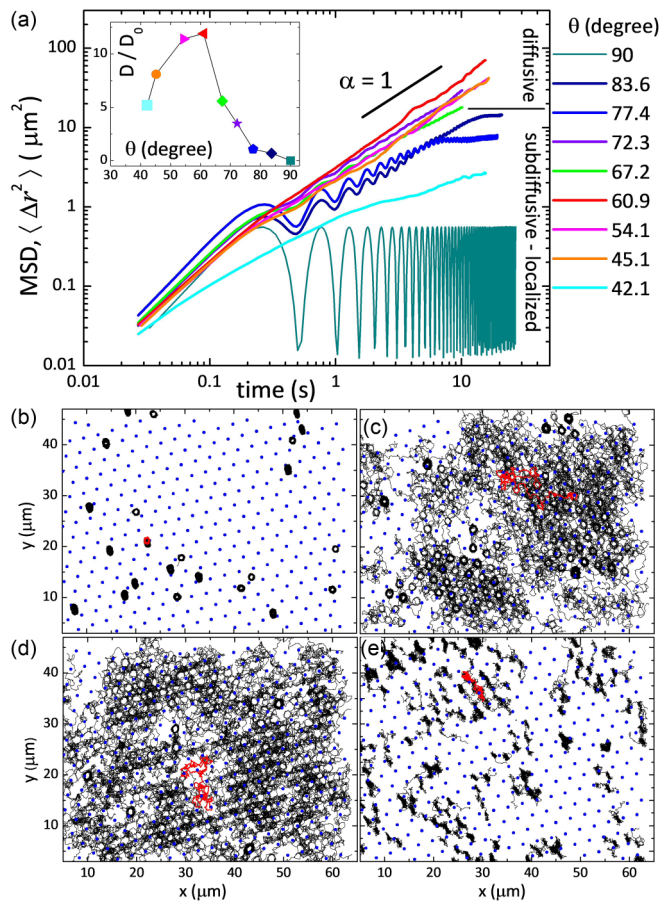
FIG. 2. (a) Mean-square displacements $\langle \Delta r^2 \rangle$ (MSDs) vs time for particles driven at different values of the precessing angle θ. For $\theta \in [42.1°, 67.2°]$ the MSD $\langle \Delta r^2 \rangle \sim t^\alpha$ is diffusive for all time ($\alpha = 1$). The inset shows the effective diffusion coefficient extracted from the data and rescaled with respect to the free diffusion above the FGF film, $D_0 = 0.125 \ \mu m^2 \, s^{-1}$ measured from independent experiments. (b)–(e) Particle trajectories when driven by a precessing field with frequency $\omega = 4\pi \, \text{rad} \, s^{-1}$ in a field of view of 2640 μm^2 (total field of view is 3120 μm^2). The precessing angles are (b) $\theta = 90°$ ($H_z = 0$), (c) $\theta = 72.2°$, (d) $\theta = 60.9°$, and (e) $\theta = 42.1°$. For all cases the amplitude of the in-plane component is $H_{xy} = 720 \ \text{A} \, m^{-1}$. The positions of the underlying magnetic bubbles are superimposed to all images, and one trajectory is highlighted in red. Corresponding videos (videos S1–S4) can be found in the Supplemental Material [50].

H_{xy} breaks this symmetry and creates a gradient along the circle. When the field rotates, the particle lags behind the minimum and is forced to move, but cannot escape from the magnetic domain. Due to the confined and periodic motion, the MSD displays a series of oscillations but does not grow with time. When $H_z > 0$, the orbital motion around the bubble becomes unstable and the particles delocalize through the lattice moving across the interstitial region [Figs. 2(c) and 2(d)]. A typical trajectory is composed by a sequence of rotational motion around a magnetic bubble, followed by random jumps between magnetic domains. While we expect that such motion would emerge in the form of a superdiffusive ($\alpha > 1$) or ballistic ($\alpha = 2$) dynamics, as observed with larger micron-size particles [41], we find a

stable diffusive motion with $\alpha = 1$ for the total measured time range. The nanoscale particles are affected by strong thermal fluctuations which randomize the process of jumping between near orbits. Thus, thermal fluctuations play a decisive role during the short time when the particle decides between competing directions along the lattice, which occurs twice during a field period [Fig. 2(c)]. The choice of the crystallographic direction during propulsion results from a dynamically symmetry breaking due to the absence of any bias in the applied precessing field.

From the slope of the MSDs we also extract an effective diffusion coefficient as $D = \lim_{t \to \infty} \langle \Delta r^2 \rangle / 4t$, which is shown in the inset of Fig. 2(a) rescaled by the free diffusion measured above the FGF in the absence of external field D_0. The particles display an enhanced diffusive dynamics, reaching the maximum value of $D = 11.9D_0$ for $\theta = 60.9°$. Finally, for angle $\theta = 42.1°$ the energy minima are so close that the particles are trapped in triangular orbits between the magnetic bubbles, and the MSD grows in a subdiffusive way, $\alpha < 1$ [Fig. 2(e)].

Further, we measure the distribution of displacement $G_s(r, t)$, which gives the probability to find a particle at position r on the plane after a lag time t. G_s represents the self-part of the van Hove correlation function [51] and, in a simple diffusive process, G_s is Gaussian, given by $G_s(r, t) = \frac{1}{4\pi Dt} \exp\left(-\frac{r^2}{4Dt}\right)$. As observed previously [21], a complex environment could alter the shape of $G_s(r, t)$, giving rise to exponential tails. It was also postulated that some systems could feature a linear MSD with a $G_s(r, t)$ composed of two Gaussians with different variances [31]. Such a situation has been treated theoretically in some works in the past with biological [52] or other systems [53], however, not many experimental examples were reported so far. Here, we find that G_s is Gaussian at a very short time $t = 0.027$ s and it broadens for $t \geqslant 5$ s while still keeping its original, Gaussian shape and central peak [Fig. 3(a)].

After testing different functional shapes, we find that our data can be well fitted by a combination of weighted Gaussians,

$$G_s(r, t) = \phi \, G_1(r, t) + (1 - \phi)G_2(r, t), \quad (2)$$

where $0 < \phi < 1$ is the fractional contribution of the two distributions, $G_{1,2}$. These are characterized by different variances and thus effective diffusion coefficients, D_1 and D_2. The presence of a mixed Gaussian distribution can be understood by considering that, after $t \sim 5$ s, the nanoparticles can be split in two populations, namely localized particles (D_1) which perform confined diffusive motion (not rotational) and do not escape from the bubbles, and the delocalized particles which stochastically switch between nearest bubbles (D_2). We use Eq. (2) to fit the experimental data for lag times $t = 5$ s and $t = 10$ s, and show in Fig. 3(b) the difference between the initial Gaussian behavior ($t = 0.027$ s) and the double Gaussian one ($t = 5$ s). From the analysis of the experimental data, we extract the effective diffusion coefficients of the two populations which are plotted in Fig. 3(d) for all cone angles $\theta \in [54.3°, 83.7°]$. The obtained values can be explained with the following arguments. For the localized orbits [Fig. 3(d) top], we find a very small effective diffusion coefficient of
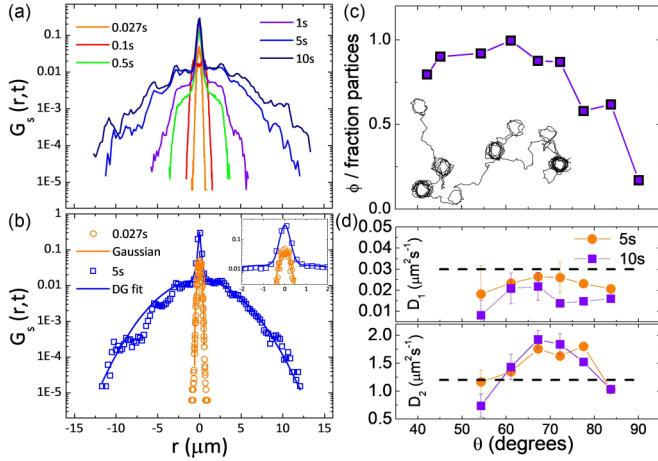
FIG. 3. (a) Probability distribution function $G_s(r,t)$ for $\theta = 83.7°$ and at different lag times t (s). (b) The distribution $G_s(r,t)$ for $\theta = 83.7°$ and at two lag times fitted with a Gaussian ($t = 0.027$ s) and with a mixed Gaussian ($t = 5$ s), Eq. (3). The top inset shows an enlargement of the central graphs. (c) Fraction $\phi = N_d/N$ of delocalized particles N_d (the bottom inset shows one trajectory) over the total number of particles N. The remaining particles perform localized orbital motion around the magnetic domains. (d) Effective diffusion coefficients D_1 and D_2 vs cone angle θ extracted from the distributions $G_s(r,t)$ at two lag times, 5 s (magenta) and 10 s (violet). The top shows D_1 for the localized particles, while the bottom graph D_2 for the delocalized ones. The dashed black lines are the estimated values as explained in the text.

the order of $D_1 = 0.02 \ \mu\mathrm{m}^2\,\mathrm{s}^{-1}$. This corresponds to the dynamics of a Brownian walker which is trapped along a thin ring, i.e., a circle of length $L = 2\pi R$ and width $\delta \sim 10$ nm (Bloch wall width). The corresponding diffusion coefficient is given by $D = \frac{L\delta}{t_d} = 0.03 \ \mu\mathrm{m}^2\,\mathrm{s}^{-1}$, where the self-diffusion time t_d can be estimated from the free diffusion coefficient D_0 as $t_d = d^2/D_0$. For these particles we are neglecting the effect of the driving field on the landscape and considering only the pinning to the BWs. Thus, they do not continuously rotate around the bubble as in the case of $\theta = 90°$, but simply display a confined diffusive behavior. As shown in Fig. 3(c), these particles represent a small fraction of the entire sample. In contrast, the fraction of delocalized particles ϕ increases as the field cone angle decreases since, as shown in Fig. S2 in the SM [50], it is directly related to the height of the potential barrier ΔE which increases with θ. Thus, the fraction of localized orbits increases with ΔE as more particles are unable to escape from the nearest bubble. For the delocalized orbits, we can estimate the effective diffusion coefficient D_2 by considering the corresponding value calculated for the random walk on isotropic lattices [54,55]. We assume that the step between two consecutive jumps is $l \sim a/2$, with a the lattice constant and the jumping time $t_s = \pi/\omega = 0.5$ s. We get $D_2 = \frac{l^2}{4t_s} = 1.2 \ \mu\mathrm{m}^2\,\mathrm{s}^{-1}$, in very good agreement with the results obtained from the distribution G_s [see Fig. 3(d) bottom]. The non-Gaussianity in our system can be also confirmed by measuring a positive non-Gaussian parameter α_2. As shown in Fig. 1 in the SM [50], we find that for all cone angles $\alpha_2 > 0$ with values $\alpha_2 \in [0.2, 4]$.
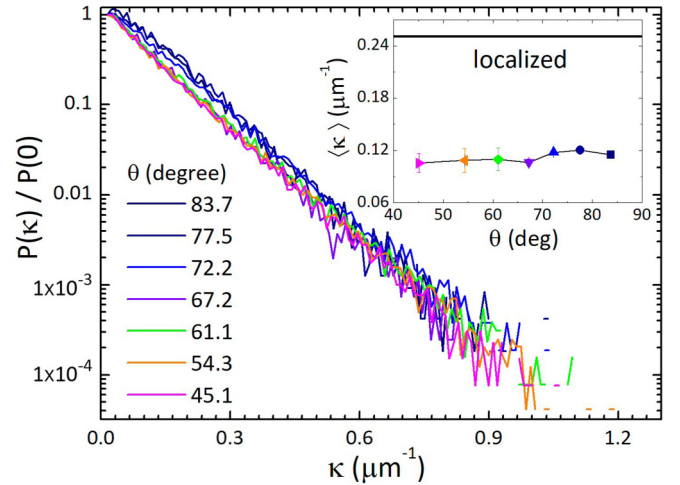

FIG. 4. Normalized probability distribution of the trajectory curvature κ for different precession angles $\theta \in [45.1°, 83.7°]$ considering only the delocalized trajectories. The inset shows the average mean curvature $\langle\kappa\rangle$ vs θ, where the continuous line is the corresponding value for the fraction of localized particles.

Finally, we analyze the particle trajectories by measuring the path curvature [56], here defined as $\kappa = |\nabla \cdot \boldsymbol{n}|/2$, where $\boldsymbol{n}$ is the unit vector normal to the direction of motion. In Fig. 4 we show the normalized probability distribution $P(\kappa)$ calculated only for the fraction of delocalized particles and plot the corresponding mean value $\langle\kappa\rangle$ in the inset. All distributions decay exponentially as $P(\kappa) \sim e^{-\kappa}$ and display similar curvatures. This enforces the fact that the delocalized particles have similar trajectories for all values of θ, which is in agreement with the similar behavior of the distributions $G_s(r,t)$. In contrast, their average curvature is lower than the curvature of the localized orbits since the latter corresponds to the smallest loop approximately equal to the bubble perimeter.

Conclusions. We have investigated the out-of-equilibrium dynamics of nanoparticles magnetically driven above a triangular lattice of ferromagnetic domains. We find that for a finite set of precession angles, the particles display a diffusive yet non-Gaussian dynamics with a linear mean-square displacement and a distribution of displacement which can be interpreted in terms of two Gaussians. These functions result from the coexistence of two types of dynamics in the system, namely confined particles performing simple diffusion around the BWs and delocalized ones. It is also tempting to interpret the statistics of our system within the framework of the continuous-time random walk, since the magnetic bubbles can be considered as trapping spots where the particles are adsorbed for a finite period of time. This indeed represents a future avenue for this work. An alternative development would be to analyze the system as a dissipative Galton board [57,58] where the magnetic bubbles behave as scattering centers. Apart from the different theoretical directions that our experimental work may open, we demonstrate the emergence of non-Gaussian diffusivity, in the field of particle transport across periodic potentials. Thus, we add another dimension to this mature yet expanding research field.

[1] G. Grüner, Rev. Mod. Phys. **60**, 1129 (1988).

[2] R. Fleischmann, T. Geisel, and R. Ketzmerick, Phys. Rev. Lett. **68**, 1367 (1992).

[3] J. Wiersig and K.-H. Ahn, Phys. Rev. Lett. **87**, 026803 (2001).

[4] J. H. Smet, K. von Klitzing, D. Weiss, and W. Wegscheider, Phys. Rev. Lett. **80**, 4538 (1998).

[5] C. Reichhardt, J. Groth, C. J. Olson, S. B. Field, and F. Nori, Phys. Rev. B **54**, 16108 (1996).

[6] S. B. Field, S. S. James, J. Barentine, V. Metlushko, G. Crabtree, H. Shtrikman, B. Ilic, and S. R. J. Brueck, Phys. Rev. Lett. **88**, 067003 (2002).

[7] J. E. Villegas, S. Savel'ev, F. Nori, E. M. Gonzalez, J. V. Anguita, R. García, and J. L. Vicent, Science **302**, 1188 (2003).

[8] S. Mühlbauer, B. Binz, F. Jonietz, C. Pfleiderer, A. Rosch, A. Neubauer, R. Georgii, and P. Böni, Science **323**, 915 (2009).

[9] C. Reichhardt, D. Ray, and C. J. O. Reichhardt, Phys. Rev. B **98**, 134418 (2018).

[10] C. Bechinger, R. Di Leonardo, H. Löwen, C. Reichhardt, G. Volpe, and G. Volpe, Rev. Mod. Phys. **88**, 045006 (2016).

[11] M. B. Hastings, C. J. Olson Reichhardt, and C. Reichhardt, Phys. Rev. Lett. **90**, 247004 (2003).

[12] J. Loehr, A. Ortiz-Ambriz, and P. Tierno, Phys. Rev. Lett. **117**, 168001 (2016).

[13] Y.-L. Wang, X. Ma, J. Xu, Z.-L. Xiao, A. Snezhko, R. Divan, L. E. Ocola, J. E. Pearson, B. Janko, and W.-K. Kwok, Nat. Nanotechnol. **13**, 560 (2018).

[14] D. Babi, C. Schmitt, and C. Bechinger, Chaos **15**, 026114 (2005).

[15] A. Yethiraj and A. van Blaaderen, Nature (London) **421**, 513 (2003).

[16] P. T. Korda, M. B. Taylor, and D. G. Grier, Phys. Rev. Lett. **89**, 128301 (2002).

[17] C. Reichhardt, C. J. Olson, and M. B. Hastings, Phys. Rev. Lett. **89**, 024101 (2002).

[18] P. Hänggi and F. Marchesoni, Rev. Mod. Phys. **81**, 387 (2009).

[19] B. Lim, V. Reddy, X. Hu, K. Kim, M. Jadhav, R. Abedini-Nassab, Y. Noh, Y. T. Lim, B. B. Yellen, and C. Kim, Nat. Commun. **5**, 3846 (2014).

[20] A. V. Arzola, M. Villasante-Barahona, K. Volke-Sepúlveda, P. Jákl, and P. Zemánek, Phys. Rev. Lett. **118**, 138002 (2017).

[21] B. Wang, S. M. Anthony, S. C. Bae, and S. Granick, Proc. Natl. Acad. Sci. USA **106**, 15160 (2009).

[22] H. Kurtuldu, J. S. Guasto, K. A. Johnson, and J. P. Gollub, Proc. Natl. Acad. Sci. USA **108**, 10391 (2011).

[23] K. He, F. B. Khorasani, S. T. Retterer, D. K. Thomas, J. C. Conrad, and R. Krishnamoorti, ACS Nano **7**, 5122 (2013).

[24] J. Kim, C. Kim, and B. J. Sung, Phys. Rev. Lett. **110**, 047801 (2013).

[25] T. O. E. Skinner, S. K. Schnyder, D. G. A. L. Aarts, J. Horbach, and R. P. A. Dullens, Phys. Rev. Lett. **111**, 128301 (2013).

[26] W. He, H. Song, Y. Su, L. Geng, B. J. Ackerson, H. B. Peng, and P. Tong, Nat Commun. **7**, 11701 (2016).

[27] J.-H. Jeon, M. Javanainen, H. Martinez-Seara, R. Metzler, and I. Vattulainen, Phys. Rev. X **6**, 021006 (2016).

[28] A. G. Cherstvy, S. Thapa, C. E. Wagner, and R. Metzler, Soft Matter **15**, 2526 (2019).

[29] R. Metzler and J. Klafter, Phys. Rep. **339**, 1 (2000).

[30] Y. Meroz and I. M. Sokolov, Phys. Rep. **573**, 1 (2005).

[31] B. Wang, J. Kuo, S. C. Bae, and S. Granick, Nat. Mater. **11**, 481 (2012).

[32] M. V. Chubynsky and G. W. Slater, Phys. Rev. Lett. **113**, 098302 (2014).

[33] R. Jain and K. L. Sebastian, J. Phys. Chem. B **120**, 3988 (2016).

[34] A. V. Chechkin, F. Seno, R. Metzler, and I. M. Sokolov, Phys. Rev. X **7**, 021002 (2017).

[35] K. C. Leptos, J. S. Guasto, J. P. Gollub, A. I. Pesci, and R. E. Goldstein, Phys. Rev. Lett. **103**, 198103 (2009).

[36] E. Weeks, J. Crocker, A. Levitt, A. Schofield, and D. Weitz, Science **287**, 627 (2000).

[37] S. M. Shell, P. G. Debenedetti, and F. H. Stillinger, J. Phys.: Condens. Matter **17**, S4035 (2005).

[38] P. Chaudhuri, L. Berthier, and W. Kob, Phys. Rev. Lett. **99**, 060604 (2007).

[39] A. V. Orpe and A. Kudrolli, Phys. Rev. Lett. **98**, 238001 (2007).

[40] M. Khoury, A. M. Lacasta, J. M. Sancho, and K. Lindenberg, Phys. Rev. Lett. **106**, 090602 (2011).

[41] P. Tierno, T. H. Johansen, and T. M. Fischer, Phys. Rev. Lett. **99**, 038303 (2007).

[42] J. M. Sancho, A. M. Lacasta, K. Lindenberg, I. M. Sokolov, and A. H. Romero, Phys. Rev. Lett. **92**, 250601 (2004).

[43] A. M. Lacasta, J. M. Sancho, A. H. Romero, I. M. Sokolov, and K. Lindenberg, Phys. Rev. E **70**, 051104 (2004).

[44] R. D. L. Hanes, M. Schmiedeberg, and S. U. Egelhaaf, Phys. Rev. E **88**, 062133 (2013).

[45] M. J. Skaug, J. Mabry, and D. K. Schwartz, Phys. Rev. Lett. **110**, 256101 (2013).

[46] C. Reichhardt and C. J. O. Reichhardt, Rep. Prog. Phys. **80**, 026501 (2017).

[47] P. Tierno, F. Sagués, T. H. Johansen, and T. M. Fischer, Phys. Chem. Chem. Phys. **11**, 9615 (2009).

[48] J. C. Crocker and D. G. Grier, J. Colloid Interface Sci. **179**, 298 (1996).

[49] R. L. Stoop, A. V. Straube, T. H. Johansen, and P. Tierno, Phys. Rev. Lett. **124**, 058002 (2020).

[50] See Supplemental Material at http://link.aps.org/supplemental/10.1103/PhysRevResearch.2.032031 for four supplemental videos as support of the experimental results, and one PDF file with two additional images, which includes Refs. [57,58].

[51] L. Van Hove, Phys. Rev. **95**, 249 (1954).

[52] E. Reister-Gottfried, S. M. Leitenberger, and U. Seifert, Phys. Rev. E **81**, 031903 (2010).

[53] L. Berthier and G. Biroli, Rev. Mod. Phys. **83**, 587 (2011).

[54] J. Machta and R. Zwanzig, Phys. Rev. Lett. **50**, 1959 (1983).

[55] R. Klages and C. Dellago, J. Stat. Phys. **101**, 145 (2000).

[56] N. T. Ouellette and J. P. Gollub, Phys. Rev. Lett. **99**, 194502 (2007).

[57] A. D. Chepelianskii and D. L. Shepelyansky, Phys. Rev. Lett. **87**, 034101 (2001).

[58] N. Chernov and D. Dolgopyat, Phys. Rev. Lett. **99**, 030601 (2007).